Noname manuscript No.
(will be inserted by the editor)

Multistability in a three-dimensional oscillator: Tori, Resonant cycles and chaos

Nataliya Stankevich · Evgeny Volkov

Received: date / Accepted: date

Abstract The emergence of multistability in a simple three-dimensional autonomous oscillator is investigated using numerical simulations, calculations of Lyapunov exponents and bifurcation analysis over a broad area of two-dimension plane of control parameters. Using Neimark-Sacker bifurcation of 1:1 limit cycle as the starting regime, many parameter islands with the coexisting attractors were detected in the phase diagram, including the coexistence of torus, resonant limit cycles and chaos; and transitions between the regimes were considered in detail. The overlapping between resonant limit cycles of different winding numbers, torus and chaos forms the multistability.

Keywords Multistability · Quasiperiodic oscillations · Chaos · Bifurcation analysis · Lyapunov exponents

PACS PACS 05.45.-a · PACS 05.45.Pq

Mathematics Subject Classification (2000) MSC 37C55 · MSC 37E45 · MSC 37E99

1 Introduction

Synchronization of nonlinear oscillations is a ubiquitous phenomenon easy to observe in nature and technics [1], [2], [3], [4], [5] but the mechanisms whereby synchronization is achieved are diverse [1]. A textbook example of synchronization is limit cycle behavior in the presence of a periodic external force. In this case Arnold tongues are observed in the period vs amplitude of external force plane. The tongues emerge from the points on the parameter plane where the limit cycle-to-external force frequency ratio is a rational number. The tongue boundaries correspond to saddle-node bifurcation lines. As a result of bifurcation a pair of cycles (stable and unstable) appears and disappears as the control parameter crosses the tongue. The Arnold tongues are surrounded by stable two-frequency quasiperiodic oscillations on the torus. Thus, the phase trajectory moves on the surface of the ergodic torus in the phase space, and the stable limit cycle appears on the torus surface exhibiting frequency locking. A recent impressive example of Arnold tongue structures embedded in quasiperiodic regions in the discrete-time Chialvo neuron model was presented in [6].

Another fundamental nonlinear phenomenon is multistability [7], [8], that is the coexistence of several attractors in the phase space, which are attained from different initial conditions. The classical structure of Arnold tongues does not assume the coexistence between the limit cycles on the torus surface and the torus.

However, in a series of papers [9], [10], [11], [12], [13], [14], [15], [16], [17], [18], [19] this kind of multistability was described. For instance, it was observed in the model of a semiconductor laser with optical injection [9], in the systems with piecewise linear elements [10], [11], for systems with delay [11], [12], [13], [14], [15] for coupled synthetic genetic ring oscillators [16], [17] and for a ring of radio-physical oscillators [18]. In [19] similar multistability was shown for a multi-mode radio-physical generator.

N. Stankevich
Department of applied cybernetics, Saint-Petersburg State University, Saint-Petersburg, Russia
Department of Radioelectronics and Telecommunications, Yuri Gagarin State Technical University of Saratov, Saratov, Russia
E-mail: stankevichnv@mail.ru

E. Volkov
Department of Theoretical Physics, Lebedev Physical Institute, Moscow, Russia

Recently a new classification of attractors was introduced based on the system behavior near the equilibrium [20], [21], [22], [23], [24]. An attractor is called a self-excited attractor if its basin of attraction intersects with any open neighborhood of a stationary state (an equilibrium); otherwise, it is called a hidden attractor. The well known Lorenz, Rössler, and Hennon systems are classical examples of self-excited attractors. For a hidden attractor, its basin of attraction is not connected with equilibria. Hidden attractors are attractors in systems without equilibria. A lot of models with hidden attractors were described in applied science [25], [26], [27], [28], [29], [30], [31]. Recently, in [32] the connection between multistability and hidden attractors has been shown.

In this paper we consider the formation of multistability resulting from the coexistence of quasiperiodic oscillations with limit cycles, and destruction of coexisting torus and cycles, in the model with hidden attractors. We use a simple dynamical system with minimal dimension of phase space ($N = 3$). In the literature there are a few examples of autonomous models with quasiperiodic dynamics [33], [34], [35]. One of them is a model generator of quasiperiodic oscillations proposed in [34]. Analysis of this model demonstrated the opportunity of *autonomous quasiperiodic* and chaotic oscillations. In [35], a model without equilibria was examined for the presence of hidden attractors. The formation of torus, families of resonance cycles and chaos observed earlier [34], [35] was confirmed and extended to include variation of the other two model parameters [36]. However, analysis of multistability, its mechanism, and bifurcation analysis have not been done and are still waiting to be addressed. This is the goal of the present study.

The paper is organized as follows. In Sect. 2, we describe the model generator of quasiperiodic regimes and determine the domain of the parameter plane where multistability may be expected. In Sect. 3, we carry out numerical integration, bifurcation analysis, demonstrate multistability and describe the main mechanisms of multistability. In Sect. 4 we present examples of multistability between chaotic attractors and between limit cycles. And finally we conclude and discuss our results in Sect. 5.

2 A model of autonomous generator of quasiperiodic oscillations. The structure of controlling parameter plane

The model generator is described by the following three-dimensional system of differential equations [34]:

$$\begin{aligned} &\ddot{x} - (z + x^2 - 0.5x^4)\dot{x} + \omega_0^2 x = 0, \\ &\dot{z} = \mu - x^2. \end{aligned} \tag{1}$$

This model is a hybrid of a generator with hard excitation, which is given by the first equation of system (1) and a relaxation oscillator, which is given by the equation for variable z. In this autonomous system relaxation z-oscillations play a role of external perturbations with respect to the two-dimensional (x,y)-oscillator. Model (1) has two specific properties: first, it has no explicit equilibrium states, and second, it exhibits symmetry with respect to the replacement[1]:

$$(x \to -x, y \to -y, z \to z). \tag{2}$$

This model has two controlling parameters. μ is a parameter responsible for the relaxation oscillator frequency; ω_0 is a parameter responsible for the frequency of the generator with hard excitation. Thus, it is most appropriate to consider the dynamics of the model in the parameter plane $(\omega_0,\ \mu)$. Figure 1 shows a chart of

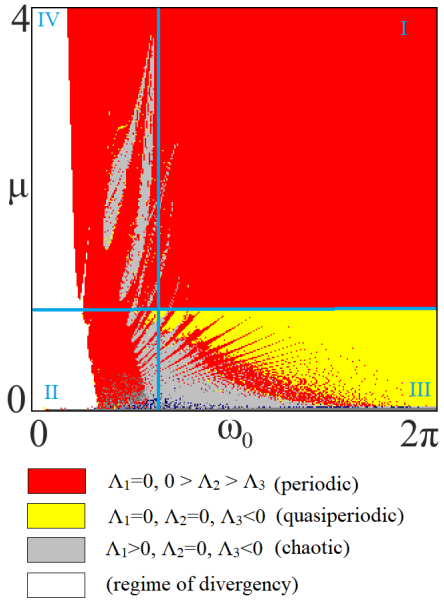

Fig. 1 Chart of Lyapunov exponents for model (1). Initial conditions for integration were the same for each point of parameter plane: x_0=0.1, y_0=0.11, z_0=0.12

Lyapunov exponents of model (1) calculated for wide

[1] Here and further we use symbol: $y = \dot{x}$

intervals of controlling parameters. This chart was constructed in the following way: parameter plane was scanned with a rather small step and for each point the full spectrum of Lyapunov exponents was calculated with the Benettin algorithm; the color of a point of parameter plane was chosen depending on the signature of the Lyapunov exponent spectrum (bottom of Fig. 1).

In the chart we can distinguish four characteristic domains: **I**, **II**, **III**, **IV**. In domain **I** ($\mu > 1$, $\omega_0 > 2$) the dominant regime is the self-oscillatory regime with period-1, the chaotic dynamics also is observed in a small areas of parameter plane. In domain **II** ($\mu < 1$, $\omega_0 < 2$) one can see a limit cycle of period-1, chaotic oscillations (which result from overlapping tongues of synchronization), very small areas of quasiperiodicity and regime of divergency. As ω_0 decreases the oscillations become more stiff and then the trajectories go to infinity. The most challenging dynamics is observed in domain **III** ($\mu < 1$, $\omega_0 > 2$): there are tongues of periodic oscillations, looking like Arnold tongues, quasiperiodic and chaotic oscillations. In domain **IV** ($\mu > 1$, $\omega_0 < 2$) self-oscillations of period-1 dominate, and there are small islands of chaotic dynamics, emerging as a result of period doubling bifurcations of the period-1 limit cycle. At small values of parameters ω_0 a regime of divergency takes place. In domain **III** the multistability is due to overlapping periodic tongues; further we are focusing on this domain.

In order to analyze and localize multistability we construct zoomed domains as charts of dynamic regimes[2] and charts of Lyapunov exponents for model (1) with different directions of scanning of the parameter plane and with the so-called continuation method of changing the initial conditions: for each new value of parameter μ the initial conditions were chosen as the final state attained for the previous value of parameter μ. The charts in Figs. 2a and 2b are constructed by scanning the parameter plane from bottom to top; and the charts in Figs. 2c and 2d, from top to bottom. The charts show a zoomed fragment of Fig. 1 corresponding to domain **III**. On all charts the Neimark-Sacker bifurcation line corresponding to the value of the parameter $\mu \approx 1$ is clearly visible.

As a result of this bifurcation, the limit cycle of period-1 loses stability creating a two-frequency torus. Along this line below the bifurcation threshold, there is a set of synchronization tongues with different winding numbers, the tongues tips lie on the bifurcation line.

[2] Chart of dynamic regimes was constructed in the same way as the chart of Lyapunov exponents, except that for each point of the parameter plane the period of oscillations was determined by the number of fixed points in the Poincaré section by plane $y = 0$

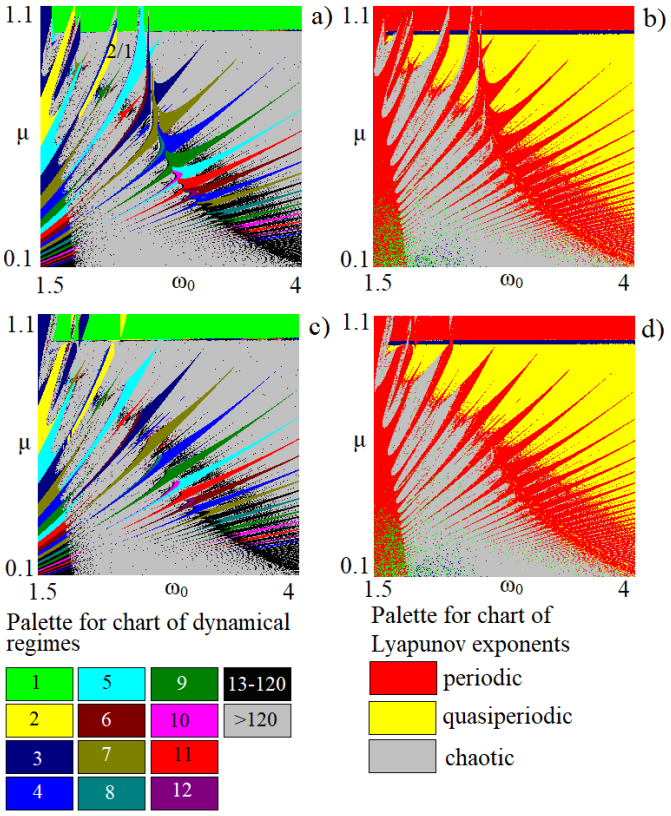

Fig. 2 a), c) chart of dynamical modes and b), d) chart of Lyapunov exponents for model (1). Charts were constructed with continuation method of changing initial conditions. Charts a), b) were constructed for scanning of parameter plane from bottom to top, and visualize tongues of periodic limit cycles. Charts c), d) were constructed for scanning of parameter plane from top to bottom and visualize quasiperiodic regimes

With a further decrease in the parameters μ and ω_0 overlapping of tongues are observed along the diagonal line $\omega_0 \sim -\mu$, and the torus is destroyed through loss of smoothness of the invariant curve. Thus, for instance, for $\mu < 0.5$ and $\omega_0 < 3$, quasiperiodic oscillations are replaced by chaotic ones.

Using the continuation method the initial conditions chosen and different scanning directions, we can visualize the coexisting regimes and roughly determine the areas of multistabilty. So, if we scan a plane from top to bottom, we show the regimes emerged as a result of the Neimark-Sacker bifurcation, and these charts are oriented to visualization of the torus. As one can see from Fig. 2a the tongue tips are surrounded by the quasi-periodic regimes on the boundary of the Neimark-Sacker bifurcation line. Comparative analysis of the charts constructed using different scanning directions the parameter plane makes it possible to detect domains of coexistence of various synchronous cycles and quasiperi-

odic oscillations. The domains of periodic regimes shown in Figs. 2a and 2b are replaced partially by the domains of quasiperiodic oscillations in Figs. 2c and 2d.

Tongues situated along the Neimark-Sacker bifurcation line have various winding numbers. For model (1) winding number can be calculated in two ways: (i) ratio of numbers of rotations of variables x and y and (ii) ratio of numbers of rotations of variables x and z. For the first case the winding number will be equal to one. The winding numbers, determined for variables x and z will be different for different tongues. If we start from the tongue of period-2 marked as 2/1 in Fig. 2a and move to the right on the parameter plane we observe the tongues with the following winding numbers: 2/1, 5/2, 3/1, 7/2, 4/1, 9/2, 5/1, 11/2, 6/1, 13/2, 7/1, etc. Inside the tongues with rotation numbers of 2/1, 3/1, 4/1, 5/1, 6/1, 7/1, 8/1, 9/1 two symmetric pairs of cycles are observed, one stable and the other unstable. Two symmetric cycles are symmetric to each other in according to replacement (2), but each of them has asymmetric structure. In Fig. 3a and 3c pairs of coexisting stable cycles of periods-3 and 4 from tongues 3/1 and 4/1 are depicted in blue and red colors, respectively. Inside the tongues with winding numbers of 5/2, 7/2, 9/2, 11/2, 13/2, etc., there is one attractor but it has symmetric structure in the phase space. These cycles represent a combination of cycles of neighboring tongues. In Fig. 3b an example of attractor with inner symmetry from tongue 7/2 is shown. In model (1) we can introduce a common winding number by doubling the numerator and denominator of the rotation number of the tongues from the first group, which will correspond to the doubling of the time realization, or these cycles will represent "united cycles", then we get a single sequence of periodic tongues with a period increasing by one: 4/2, 5/2, 6/2, 7/2, 8/2, etc. and this structure will correspond to the period-adding structure.

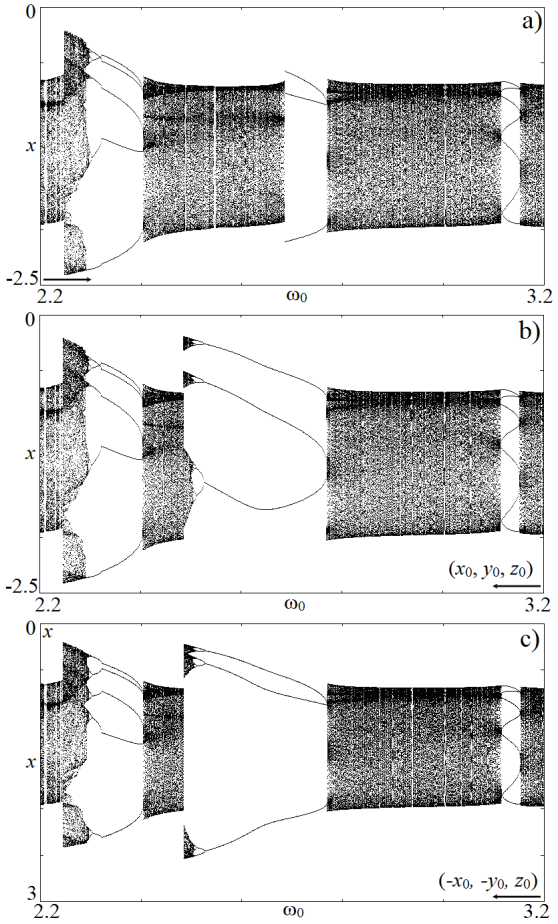

Fig. 4 Bifurcation trees for model (1) in the Poincaré section by plane $y = 0$. Trees were constructed with continuation method of changing of initial conditions, and with different starting initial conditions and different scanning directions of the parameter: a) random starting initial condition with scanning direction from left to the right; b) random starting initial condition (x_0, y_0, z_0) with scanning direction from the right to the left; c) symmetric starting initial condition $(-x_0, -y_0, z_0)$ with scanning direction from the right to the left

3 Multistability

3.1 Numerical integration dependent on one parameter

To clarify the mechanism behind the coexistence of limit cycles and a torus, we consider in detail the arrangement of three neighboring periodic tongues. For example, let us take the most prominent periodic tongues with periods of 5, 3 and 7.

Figure 4 shows the bifurcation trees in the Poincaré section by plane $y = 0$ constructed for random, symmetric, starting initial conditions and the two scanning direction for the parameter interval indicated by arrows in the plots. The considered ω_0 interval includes regions with period-5, 3, 7 limit cycles and the quasi-periodic regimes.

Let us examine how the dynamics varies with decreasing ω_0. For $\omega_0 = 3.2$ a two-frequency quasiperiodic oscillations are observed [3]. At $\omega_0 \approx 3.153$ a limit cycle of period-7 appears, then at $\omega_0 \approx 3.117$ the limit cycle disappears and the torus emerges again. A further decrease in ω_0 to $\omega_0 \approx 2.769$ gives rise to two limit cycles of period-3, which can be reached from initial conditions symmetric with respect to replacement (2). As seen in

[3] If we consider the bifurcation tree we cannot distinguish between quasiperiodic and chaotic oscillations, but using the charts of Lyapunov exponents in Fig. 2 we can see that for mentioned parameters there are quaisperiodic oscillations with two zero Lyapunov exponents

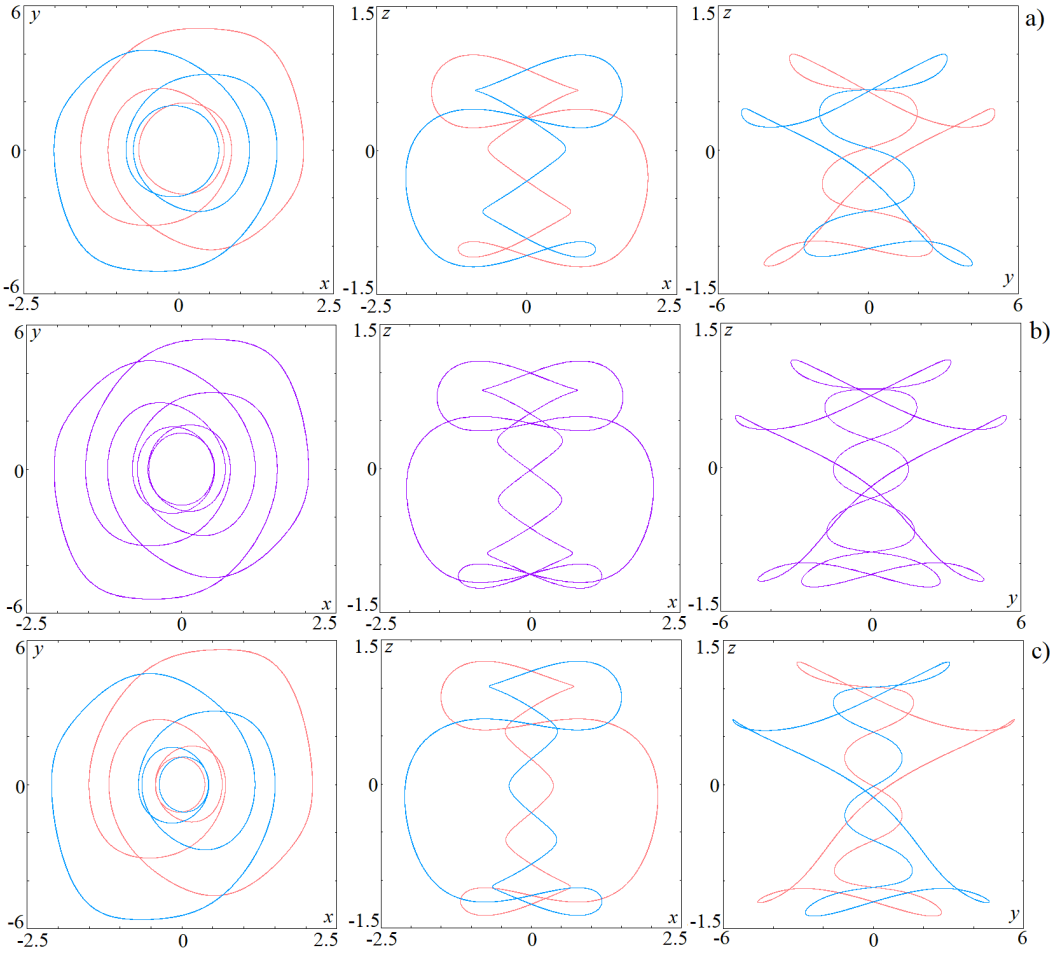

Fig. 3 Two-dimensional projections of phase portraits of model (1) from neighboring tongues of limit cycles a) a pair of cycles of period-3, $\mu = 0.8$, $\omega_0 = 2.75$; b) a single cycle of period-7, $\mu = 0.7$, $\omega_0 = 2.9$; c) a pair of cycles of period-4, $\mu = 0.6$, $\omega_0 = 2.95$. Red and blue lines correspond to coexisting cycles

Fig. 4b and 4c, these two cycles of period-3 undergo a sequence of period-doubling bifurcations with decreasing ω_0, resulting in the appearance of two coexistent chaotic attractors. At $\omega_0 \approx 2.48$, the chaotic attractors collapse and quasiperiodic oscillations are observed again. In case if the scan direction is reversed (Fig. 4a), we see that, in addition to the cycles, a two-frequency torus emerges in a system at $\omega_0 \approx 2.6853$. At lower ω_0, the torus coexists with all the dynamic regimes born on the basis of period-3 limit cycles.

As ω_0 decreases further, two-frequency quasiperiodic oscillations are observed and at $\omega_0 \approx 2.4$ a limit cycle of period 5 arises, which loses amplitude symmetry in pitchfork bifurcation and splits to a pair of coexisting cycles. Each of the limit cycles undergoes a cascade of period doubling bifurcations leading to chaos. Interestingly, in this window of periodicity, the limit cycles do not coexist with the torus , as it was with the limit cycles of period-3. At $\omega_0 \approx 2.24533$ the chaotic attractor disappears via a crisis and a two-frequency torus emerges in the system again as ω_0 goes below 2.24533.

3.2 One- and two-parametric numerical bifurcation analysis

In Fig. 5a, the bifurcation diagrams for the limit cycles drawn in Fig. 4 were generated with XPP AUTO [37]. In calculations, the scale of the parameter axis is the same as in Fig. 4. In Fig. 5b the zoomed fragment demonstrating the structure of the tongue of the limit cycle of period-7 is shown. In order to distinguish between different cycles, we use different colors, which are denoted in the bottom of Fig. 5.

If we decrease ω_0 starting from the right side of Fig. 5a, we can see the same bifurcations as those observed with the bifurcations trees. First, one can see the birth of the limit cycle of period-7. The domain of existence of limit cycle of period-7 is bounded from

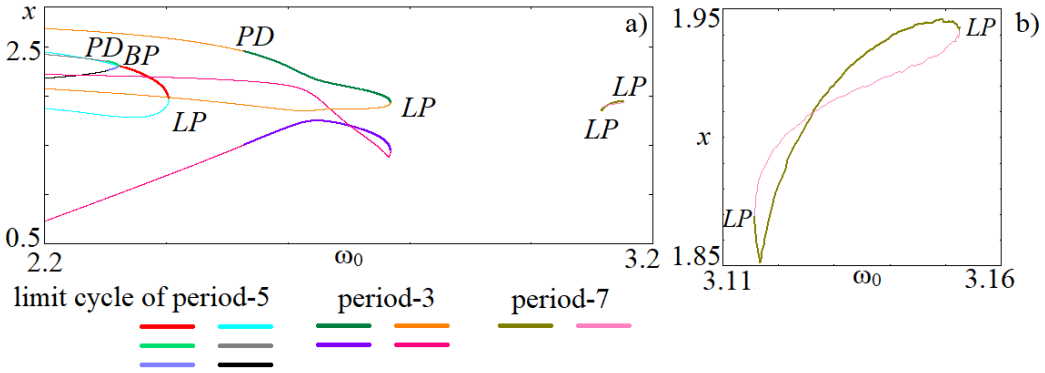

Fig. 5 Bifurcation diagrams for model (1). Diagrams were calculated using software package XPP AUTO for the limit cycles of period-5, -3, -7, for the same parameters as in Fig. 4, $\mu = 0.8$. LP is point of saddle-node bifurcation, BP is point of symmetry-break bifurcation, PD is point of period-doubling bifurcation (in order to keep figure simple stable branches after period doubling bifurcation are not shown)

both sides by the saddle-node bifurcations (LP). At $\omega_0 = 3.153$ a pair of cycles (stable and unstable) is born via a saddle-node bifurcation; at $\omega_0 = 3.117$ the second saddle-node bifurcation occurs and both cycles disappear.

With a further decrease in ω_0 the limit cycle of period-3 emerges. Choosing symmetric initial conditions according to (2), we reveal two cycles. In Fig. 5a the stable cycles for symmetric initial conditions are depicted in green and violet; and unstable ones, in orange and pink. The saddle node bifurcations (LP) at $\omega_0 = 2.769$ result in the appearance of two pairs of stable-unstable limit cycles, in agreement with the simulations shown in Fig. 4. Thereafter, the stable cycles lose stability via period doubling bifurcation (PD) at $\omega_0 = 2.527$. These unstable cycles persist with further decreasing ω_0 until the oscillations become relaxation ones and the trajectories go to infinity.

Bifurcation analysis was carried out for the limit cycle of period-5. In Fig. 5a the stable and unstable cycles are given in red and turquoise, respectively. In this case one pair of stable-unstable cycles is born as a result of saddle-node bifurcation at $\omega_0 = 2.404$ (LP). When ω_0 decreases to $\omega_0 = 2.322$, the stable limit cycle of period-5 undergoes symmetry-breaking bifurcation (BP) and the cycle splits into two symmetric to each other stable limit cycles of period-5 (see Fig. 5a). The further evolution of period-5 cycles is similar to that of limit cycles of period-3: it is a period-doubling cascade leading to chaos.

In Fig. 6 the two-parametric bifurcation diagram in the (ω_0, μ) plane generated with the software package XPP AUTO is shown. Solid lines depict the saddle-node bifurcation lines: red lines (l_5^1, l_5^2, l_5^3) stand for period-5 limit cycle, violet lines (l_3^1, l_3^2, l_3^3), for period-3 limit cycles, and olive lines (l_7^1, l_7^2, l_7^3), for period-7 limit

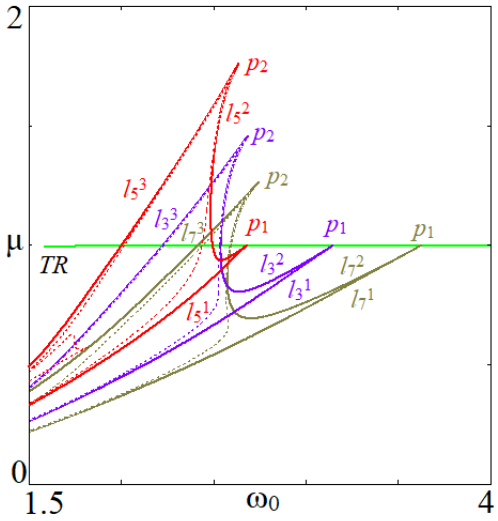

Fig. 6 Two-parametric bifurcations diagram for model (1). Solid red, violet and olive lines correspond to the saddle-node bifurcations of the cycles 5, 3, 7; dashed red, violet and olive lines correspond to the period-doubling bifurcations of the cycles 5, 3, 7. p_1, p_2 are special points of the saddle-node bifurcation lines of each cycle. Green solid line is line of Neimark-Sacker bifurcation for the limit cycle of period-1 (TR)

cycles; dashed lines depict the period-doubling bifurcation. Green solid line (TR) is the line of Neimark-Sacker bifurcation for the limit cycle of period-1, the torus is below this line. The saddle-node bifurcation lines for each limit cycle intersect at two points marked as p_1, p_2. The p_1 point is on the line of Neimark-Sacker bifurcation, corresponding to the line $\mu = 0.994$, along which tips of the tongues of limit cycles are distributed, which makes the picture look like Arnold tongues of synchronization. The second special point (p_2) is situated above the Neimark-Sacker bifurcation line, and for different tongues these points are distributed along the

line over the interval range of ω_0 (2.6-2.75). Inside of each domain bounded by saddle-node bifurcation there are lines of period doubling bifurcation. These lines are very close to the line of saddle-node bifurcation except the areas near the points p_1. It means that the limit cycle which occur as a result of saddle-node bifurcation persists in a small domain of the parameter plane, and this cycle undergoes bifurcations with the formation of chaotic attractors. But the line of period doubling bifurcation does not come close to the special point p_1. This configuration of bifurcation lines forms the picture of the tongues of periodicity similar to classical Arnold tongues of synchronization (see Figs. 1, 2a and 2b). All the lines of saddle-node bifurcation l_2 that start from point p_1, first go downward as ω_0 decreases, but then tend upward to special point p_2 and there the tongues overlap. This overlapping tongues result in the multistability between limit cycles and quasiperiodic oscillations born as a result of Neimark-Sacker bifurcation. When the limit cycle loses stability an unstable cycle can exist and it can form a complex structure of phase space allowing the coexistence of different stable attractors. Below we consider such structures.

3.3 Basins of coexisting attractors and the evolution of the invariant curves

Numerical bifurcation analysis allows us to identify the bifurcations of cycles; however, only direct numerical integration can be used to locate and analyze the torus. Let us consider the detailed evolution of the Poincaré sections during torus formation and destruction, taking into account its coexistence with limit cycles.

The discrete fixed points in Poincaré section correspond to the limit cycle in the phase space. The closed invariant curve in the Poincaré section corresponds to the torus in the phase space, whereas a chaotic attractor generates a Poincaré section with a complex structure. This classification of dynamic regimes was also verified by the analysis of the Lyapunov exponents spectrum.

Below we will consider two routes towards torus destruction, one proceeding through synchronization and the other, through crisis of torus [38]. They differ in details of evolution of the torus invariant curve:
(i) synchronization on the torus surface is associated with saddle-node bifurcations. When a bifurcation occurs, a pair of limit cycles (stable and unstable) are born. Before bifurcation the phase trajectory is condensed in the vicinity of each fixed point. Thus, before the bifurcation we observe *smooth turns* of invariant curve near the areas with high density of the phase points;
(ii) torus undergoes crisis, which means a collision of the phase trajectory with the basin of attraction of a coexisting regime, or with some unstable cycle. In this case invariant curve breaks down as a result of smoothness loss, and before the crisis *sharp bends* of the invariant curve are observed.

Let us consider the location of limit cycle fixed points and invariant curve evolution for model (1). Shown in Figs. 7-9 are phase portraits in Poincaré section calculated for the attractors located in different tongues presented in Fig. 6. We fix parameter $\mu = 0.8$ (as in calculations of the bifurcation trees and diagrams in Figs. 4 and 5) and investigate transitions between quasiperiodic and periodic regimes.

First, we consider in detail the structure of the invariant curve near the tongue of period-3 limit cycles, because in this tongue multistability is clearly observed (Fig. 4). This tongue is marked by three critical events: a) saddle-node bifurcation, $\omega_0 = 2.769$; b) torus appearance in addition to limit cycles, $\omega_0 \approx 2.6853$; and c) destruction of chaotic attractors coexisting with the torus, $\omega_0 \approx 2.49$. In Fig. 7 three corresponding phase portraits in the Poincaré section are presented.

In Fig. 7a the phase portraits in Poincaré section for neighboring values of ω_0 just before and after bifurcation are shown. The invariant curve before saddle-node bifurcation at $\omega_0 = 2.77$ and the fixed points of two coexisting limit cycles born by bifurcation at $\omega_0 = 2.768$ are given in red, black and green, respectively. These points correspond to the dynamics close to the right side of the tongue in Fig. 2. This saddle-node bifurcation line corresponds to the synchronization on the torus: before bifurcation we observe the formation of smooth turns where the phase trajectory condenses near the fixed points. Note, that the number of smooth turns is equal to the number of fixed points for the two coexisting limit cycles of period-3 (Fig. 7a). Thus, for the limit cycles of period-3, torus corresponds to the "united cycle" of period-6.

Let us now consider the invariant curve structure for coexisting torus and limit cycles of period-3. As can be seen in Fig. 7a, two limit cycles emerges on the surface of the torus at $\omega_0 = 2.768$, resulting in six smooth turns of the invariant curve. For $2.6853 < \omega_0 \leq 2.768$, only two limit cycles of period-3 coexist, and at $\omega_0 = 2.6853$ torus is added. In Fig. 7b, the phase portraits of two coexisting period-3 cycles in the Poincaré section are given along with the basins of their attraction (red, dark blue) and the basin of torus (yellow). The torus invariant curve has now five sharp bends instead of the six smooth turns. The fixed points are located in the center of their basins of attraction. The torus undergoes crisis after the invariant curve touches basins of attraction of limit cycles.

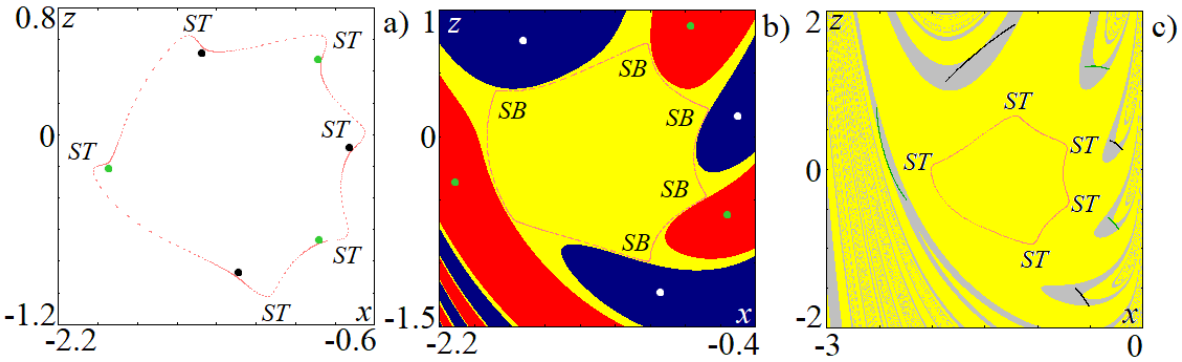

Fig. 7 Phase portraits in the Poincaré section by plane $y = 0$ in the vicinity of the limit cycles of period-3, $\mu = 0.8$ a) for two neighboring points before and after saddle-node bifurcation, $\omega_0 = 2.77$ (torus, red invariant curve), $\omega_0 = 2.768$ (two period-3 limit cycles, black and green fixed points); b) coexisting attractors in the vicinity of crisis of torus, $\omega_0 = 2.682$ (torus, red invariant curve; cycle, white and green fixed points); c) coexisting attractors in the vicinity of crisis of chaos, $\omega_0 = 2.49$ (torus, red invariant curve; chaos, black and green dots). Basins of attraction of coexisting attractors: yellow is basin of attraction of torus; red and dark blue are basins of coexisting period-3 cycles; grey is basin of two chaotic attractors. *ST* is smooth turns, *SB* is sharp bends

With a further decrease in ω_0 both limit cycles undergo a cascade of period-doubling bifurcations with the formation of two chaotic attractors. In Fig. 7c the phase portraits of coexisting attractors and their basins of attraction are shown. Yellow color marks the basin of attraction of torus, gray color marks the basin of attraction of both chaotic attractors. The invariant curve becomes smoother, and five smooth turns are visible on it. The basins of attractions have a complex fractal structure. Fig. 7c corresponds to the crisis of chaotic attractors, phase trajectories of chaotic attractors (green and black lines in Fig. 7c) touch the boundary of the basin of attraction of the torus.

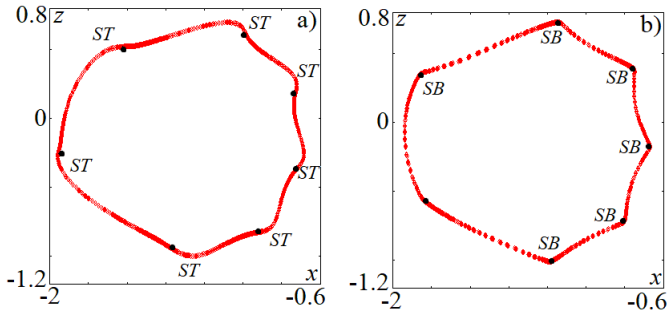

Fig. 8 Phase portraits in the Poincaré section by plane $y = 0$ for two neighboring points for the limit cycle of period-7, $\mu = 0.8$, a) before and after saddle-node bifurcation, $\omega_0 = 3.15$ (torus, red invariant curve), $\omega_0 = 3.155$ (cycle, black fixed points); b) before and after torus crisis, $\omega_0 = 3.114$ (torus, red invariant curve), $\omega_0 = 3.116$ (cycle, black fixed points). *ST* is smooth turns, *SB* is sharp bends

Next, we go to considering the tongue with the period-7 cycle. Its structure for $\mu = 0.8$ is simpler because both boundaries are saddle-node bifurcations and no coexisting attractors are present. However, the transition between the torus and the cycle at these boundaries are different. In Fig. 8a two phase portraits are shown for two close values of ω_0, which, however, are on different sides of the saddle-node bifurcation point. The invariant curve at $\omega_0 = 3.15$ is given in red and the fixed points of the limit cycle at $\omega_0 = 3.155$ are blacks. As mentioned above the condensation of phase trajectory takes place near limit cycle before saddle-node bifurcation. As a result smooth turns in the invariant curve near fixed points of the limit cycle are observed. Their number is equal to the winding number of the limit cycle arising via saddle-node bifurcation. The left boundary of the tongue of the period-7 limit cycle is also a line of the saddle-node bifurcation; two phase portraits in the Poincaré section for two adjacent values ω_0 are shown in Fig. 8b. In this case sharp bends of the invariant curve rather then smooth turns are observed reflecting the difference between torus-cycle and cycle-torus transitions. Note that the number of sharp bends is less then the winding number of the limit cycle by one; so, for the period-7 cycle it equals six.

In Fig. 9 the transitions of period-5 limit cycle are shown. For period-5 limit cycle there are also two critical events: saddle-node bifurcation and chaotic attractor breakdown. At $\omega_0 = 2.406$, synchronization is observed again and the limit cycle of period-5 emerges via saddle-node bifurcation (Fig. 9a); the five smooth turns of the invariant curve correspond to the five fixed points of the new limit cycle of period-5. In this case there is no coexistence of attractors. Instead, as ω_0 decreases, the limit cycle undergoes pitchfork symmetry breaking bifurcation followed by a cascade of the period-

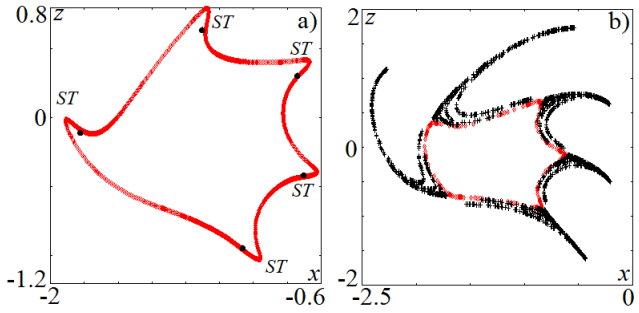

Fig. 9 Phase portraits in the Poincaré section by plane $y = 0$ for two neighboring points for the limit cycle of period-5, $\mu = 0.8$, a) before and after saddle-node bifurcation, $\omega_0 = 2.402$ (torus, red invariant curve), $\omega_0 = 2.406$ (cycle, black fixed points); b) before and after crisis of chaos, $\omega_0 = 2.245$ (chaos, black dots), $\omega_0 = 2.2415$ (torus, red invariant curve). ST is smooth turns

doubling bifurcations leading to chaos. Thereafter the chaotic attractor disappears via crisis and quasiperiodic oscillations resume. In Fig. 9b the Poincaré section for close values of ω_0 are shown, before and after crisis of chaotic attractor. Black and red points correspond to the chaotic attractor and torus, respectively.

Thus, the mechanism of multistability formation can be formulated in the following way: the boundaries of tongues of periodic regimes are the three lines of the saddle-node bifurcations (see Fig. 6, l_n^1, l_n^2, l_n^3) [4]. However, only one of these boundaries corresponds to the line of saddle-node bifurcation on the torus (l_n^1) where limit cycle emerges via synchronization. Inside the tongues pitchfork and period-doubling bifurcations of the cycles lead to chaotic regimes, which undergo crisis due to conversion to quasiperiodic regimes. In the parameter plane the tongues of periodic regimes are overlapping with one another resulting in remarkable multistability.

4 Other cases of multistability

Apart from the above presented multistability, model (1) demonstrates the coexistence of other pairs of attractors if μ changes. As μ decreases, chaotic dynamics arise through the loss of smoothness of the invariant curve. In contrast, for $\mu > 0.994$ the period-1 limit cycle dominates and serves as the base for torus formation. Below we present two examples of multistability between chaotic regimes and of unusual coexistence of limit cycles.

[4] n is a winding number of tongue

4.1 Coexistence of chaotic attractors

First, let us consider $\mu = 0.6378$ at which the torus invariant curve losses smoothness.

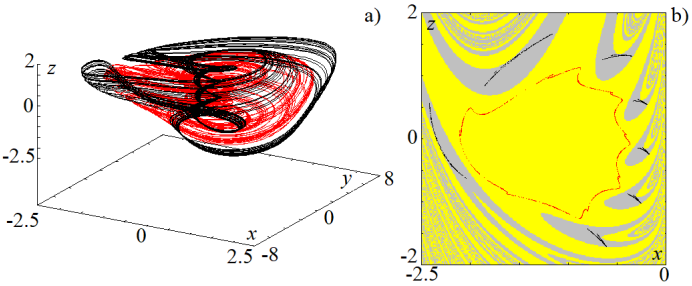

Fig. 10 a) 3D phase portraits and b) Phase portraits of coexisting chaotic attractors in the Poincaré section by plane $y = 0$ at $\mu = 0.6378$ and $\omega_0 = 2.55$ (red and black dots, respectively) and their basins of attraction (yellow and gray color, respectively)

Figure 10 shows the Poincaré sections of two coexisting chaotic attractors at $\mu = 0.6378$ and $\omega_0 = 2.55$. The first emerges via a cascade of period doubling bifurcations of the period-7 limit cycle (black color in Fig. 10); and the other, via loss of the torus invariant curve smoothness (red color in Fig. 10). For each attractor the full spectrum of Lyapunov exponents was calculated. For the chaotic attractor resulting from destruction of the invariant curve, the Lyapunov exponents are as follows: $\Lambda_1 = 0.017$, $\Lambda_2 = 0.0$, $\Lambda_3 = -0.147$; and for the chaotic attractor that appeared as a result of period-doubling bifurcations: $\Lambda_1 = 0.051$, $\Lambda_2 = 0.0$, $\Lambda_3 = -0.446$. The basins of attraction of the chaotic attractors were constructed from analysis of the largest Lyapunov exponent (see Fig. 10b). Yellow color corresponds to the basin of chaotic attractor originating from the torus. The basin of attraction of the chaotic attractor originating from the period-7 limit cycle is marked by grey color. The basins have complex fractal structure similar to that presented above in Fig.7c for coexisting torus and chaos.

4.2 Multistability without torus

For $\mu > 0.994$ (above the green line in Fig. 2) model (1) demonstrates stable period-1 limit cycle over a large interval of ω_0. The quasiperiodic oscillations are observed normally at smaller μ; however, Fig. 6 shows that two lines of saddle-node bifurcation (l_n^2, l_n^3) bounding the limit cycles get into the region above the green line providing for overlapping between synchronization tongues and period-1 cycle. Dynamics inside the tongues are

complex. It is similar to the cycle evolution described above but without torus.

As a typical example, in Fig. 11a the bifurcation trees constructed for different initial conditions are shown. At $\omega_0 = 2.493$ the period-5 limit cycle appears, then with decreasing ω_0 this cycle undergoes a pitchfork bifurcation and period doubling bifurcations leading to the emergence of a chaotic attractor. At $\omega_0 \approx 2.423$ chaotic attractor disappears via crisis. Throughout the ω_0 interval this complex attractor shares phase space with the simple period-1 limit cycle (green line in Fig. 11a). Fig. 11b shows that in phase space period-1 limit cycle is within the period-5 limit cycle. The basins of the coexisting attractors (Fig. 11c) have a complex fractal structure and are similar to the basins of the coexisting torus and chaos in Fig. 7c and to the basisns of two chaotic regimes in Fig. 10b. Note that the basin of the period-5 limit cycle is significantly smaller than the basin of the period-1 limit cycle.

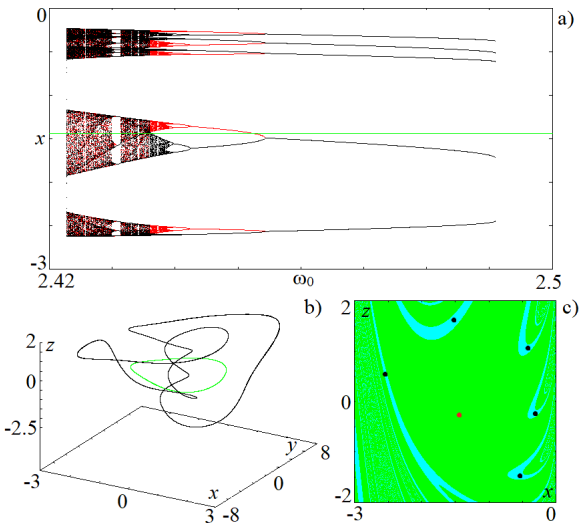

Fig. 11 a) Bifurcation trees for model (1) in the Poincaré section by plane $y = 0$. Trees were constructed with continuation method of changing of initial conditions, and with different initial conditions, $\mu = 1.029$; b) 3D phase portraits and c) Phase portraits in the Poincaré section of coexisting period-1 and period-5 limit cycles by plane $y = 0$ at $\mu = 1.029$, $\omega_0 = 2.465$ (red and black points) and its basins of attraction (green and turquoise color, respectively)

5 Conclusions

The simplest three-dimensional dynamical model of radiophysical oscillator [34], which demonstrates the absence of equilibrium and presence of hidden attractors, has been used to study multistability over a broad area of parameters. Torus formation resulting from hybridization of the well-known two-dimensional generator with hard excitation with an additional slow relaxation variable stimulates the appearance of a family of resonant cycles and chaos.

However, the detailed mechanisms of transitions between the attractors have not been addressed previously. In this work we focused on the study of the dynamics in domains of parameter space where several stable attractors - torus, limit cycles differing in winding numbers, and chaos, - may coexist in pairs making thereby all variants of the coexistence. Bifurcation analysis in combination with calculations of the Lyapunov exponent spectrum allowed us to detect the boundaries of attractor stability and reveal multistability.

The boundaries of the tongues of periodic regimes are formed by three lines of saddle-node bifurcations, only one of which corresponds to the line of saddle-node bifurcation on the torus. Transformation of the regimes inside the tongues depends on the winding number which, in turn, is controlled by parameter μ. In particular, inside the tongue with two period-3 cycles, there is a sequence of period-doubling bifurcations of cycles resulting in chaotic attractors, which undergo crisis followed by torus formation. We found that the back transition from torus to period-3 cycle takes place for different parameter values and the mechanism behind is torus crisis after the cycle basin touches the torus invariant curve.

Similarly, we clarified the mechanisms of transformations inside the other tongues and presented the illustrations of coexistence between quasiperiodic and periodic (or chaotic) oscillations, as well as between two different chaotic attractors. Special attention is given to multistability in the region where μ is above the line of torus formation. In this region coexistence of period-1 limit cycle and other limit cycles of different periods, as well as the creation of chaos inside the synchronization tongues have been observed and illustrated for the tongue with the period-5 cycle.

This simple model may serve as a paradigmatic example of how to study multistability in composite nonlinear oscillators, as well as in coupled identical oscillators with different versions of self-organized quasiperiodicity. In particular, this approach can be important for the modeling of biological intracellular processes when the oscillating regime is modulated by some other slow process. Such a situation can not be considered within the limits of a well-known "reaction-diffusion" approach. For example, the recent great interest to the dynamic behavior of the fast synthetic genetic oscillators inside the cell with slow metabolic reactions requires the development of an integrated model [17].

Acknowledgements This work was supported by Russian Foundation for Basic Research (Grant No. 17-302-50014). Authors thank S.P. Kuznetsov for the helpful discussions and R. Volkova for the editorial efforts.

Conflicts of Interest

The authors declare no conflict of interest.

References

1. Pikovsky A., Rosenblum M., & Kurths J., Synchronization: a universal concept in nonlinear sciences (Vol. 12). Cambridge university press. (2003)
2. Anishchenko V.S., Vadivasova T.E., Strelkova G.I., Synchronization of Periodic Self-Sustained Oscillations. In: Deterministic Nonlinear Systems. Springer Series in Synergetics. Springer, Cham. (2014)
3. Shilnikov A., Shilnikov L., Turaev D., On some mathematical topics in classical synchronization. A tutorial., Int. J. Bif. Chaos. 14, 2143-2160 (2004)
4. Kuznetsov A.P., Stankevich N.V., Turukina L.V., Coupled van der PolDuffing oscillators: Phase dynamics and structure of synchronization tongues, Physica D, 238, 1203-1215 (2009)
5. Bezruchko B.P., Prokhorov M.D., & Seleznev, Y.P., Oscillation types, multistability, and basins of attractors in symmetrically coupled period-doubling systems, Chaos, Solitons & Fractals, 15, 695-711 (2003)
6. Wang F., Cao H., Mode locking and quasiperiodicity in a discrete-time Chialvo neuron model, Communications in Nonlinear Science and Numerical Simulation, 56, 481-489 (2018)
7. Feudel U., Complex dynamics in multistable systems, International Journal of Bifurcation and Chaos, 18, 1607-1626 (2008)
8. Pisarchik A.N., & Feudel U., Control of multistability, Physics Reports, 540, 167-218 (2014)
9. Wieczorek S., Krauskopf B., & Lenstra D., Mechanisms for multistability in a semiconductor laser with optical injection, Optics Communications, 183, 215-226 (2000)
10. Zhusubaliyev Z.T., Mosekilde E., Multistability and hidden attractors in a multilivel DC/DC converter, Mathematics and Computers in Simulation, 109, 32-45 (2015)
11. Zhusubaliyev Z.T., Mosekilde E., Rubanov V.G., Nabokov R.A., Multistability and hidden attractors in a relay system with hysteresis, Physica D, 306, 6-15 (2015)
12. Churilov A.N., Medvedev A., Zhusubaliyev Z.T., Impulsive Goodwin oscillator with large delay: periodic odcillations, bistability, and attractors, Nonlinear Analysis: Hybrid Systems, 21, 171-183 (2016)
13. Zhusubaliyev Z.T., Mosekilde E., Churilov A.N., Medvedev A., Multistability and hidden attractors in an impulsive Goodwin oscillator with time delay, The European Physical Journal. Special Topics, 224, 1519-1539 (2015)
14. Rosin D.P., Callan K.E., Gauthier D.J., & Schöll E., Pulse-train solutions and excitability in an optoelectronic oscillator, EPL (Europhysics Letters), 96, 34001 (2011)
15. Balakin M.I., Ryskin N.M., Bifurcational mechanism of formation of developed multistability in a van der Pol oscillator with time-delayed feedback, Rus. J. Nonlin. Dyn., 13, 151164 (2017) (Russian)
16. Hellen E. H., Volkov E., Flexible dynamics of two quorum-sensing coupled repressilators, Physical Review E, 95, 022408 (2017)
17. Hellen E. H., Volkov E., How to couple identical ring oscillators to get Quasiperiodicity, extended Chaos, Multistability and the loss of Symmetry, Communications in Nonlinear Science and Numerical Simulation, 62, 462-479 (2018).
18. Dvorak A., Astakhov V., Perlikowski P., Kapitaniak T., Nonlinear resonance and synchronization in the ring of unidirectionally coupled Toda oscillators, The European Physical Journal Special Topics, 225, 2635-2643 (2016)
19. Astakhov S., Astakhov O., Astakhov V., & Kurths J., Bifurcational Mechanism of Multistability Formation and Frequency Entrainment in a van der Pol Oscillator with an Additional Oscillatory Circuit, International Journal of Bifurcation and Chaos, 26, 1650124 (2016)
20. Leonov G.A., Kuznetsov N.V., Vagaitsev V.I., Localization of hidden Chua's attractors, Physics Letters A, 375, 2230-2233 (2011)
21. Leonov G.A., Kuznetsov N.V., Hidden attractors in dynamical systems. From hidden oscillations in Hilbert-Kolmogorov, Aizerman, and Kalman problems to hidden chaotic attractors in Chua circuits, Int.J.Bif.Chaos, 23, 1330002 (2013)
22. Leonov G.A., Kuznetsov N.V., Mokaev T.N., Homoclinic orbits, and self-excited and hidden attractors in a Lorenz-like system describing convective fluid motion, Eur.Phys.J. Special Topics, 224, 1421-1458 (2015)
23. Kuznetsov N.V., Hidden attractors in fundamental problems and engineering models. A short survey, Lecture Notes in Electrical Engineering, 371, 13-25 (2016)
24. Kuznetsov N.V., Leonov G.A., Mokaev T.N., Prasad A., Shrimali M.D., Finite-time Lyapunov dimension and hidden attractor of the Rabinovich system, Nonlinear dyn (2018) https://doi.org/10.1007/s11071-018-4054-z
25. Zhao H., Lin Y., & Dai Y., Hidden attractors and dynamics of a general autonomous van der PolDuffing oscillator. International Journal of Bifurcation and Chaos, 24, 1450080 (2014)
26. Kengne J., Njitacke Z.T., & Fotsin H.B., Dynamical analysis of a simple autonomous jerk system with multiple attractors. Nonlinear Dyn, 83, 751-765 (2016)
27. Kuznetsov N.V., Leonov G.A., Yuldashev M.V., Yuldashev R.V., Hidden attractors in dynamical models of phase-locked loop circuits: limitations of simulation in MATLAB and SPICE, Commun Nonlinear Sci Numer Simulat, 51, 39-49 (2017)
28. Chen G., Kuznetsov N.V., Leonov G.A., Mokaev T.N., Hidden attractors on one path: Glukhovsky-Dolzhansky, Lorenz, and Rabinovich systems, Int.J.Bif.Chaos, 27, 1750115 (2017)
29. Xu Q., Zhang Q., Bao B., & Hu Y., Non-Autonomous Second-Order Memristive Chaotic Circuit. IEEE Access, 5, 21039-21045 (2017)
30. Danca M.-F., Kuznetsov N.V., Hidden chaotic sets in a Hopfield neural system, Nonlinear dynamics, Chaos, Solitons & Fractals, 103, 144-150 (2017)
31. Danca M.-F., Fečkan M., Kuznetsov N.V., Chen G., Complex dynamics, hidden attractors and continuous approximation of a fractional-order hyperchaotic PWC system, Nonlinear dyn, 91, 2523-2540 (2018)
32. Dudkowski D., Jafari S., Kapitaniak T., Kuznetsov N.V., Leonov G.A., & Prasad A., Hidden attractors in dynamical systems, Physics Reports, 637, 1-50 (2016)
33. Anishchenko V.S., Nikolaev S.M., Generator of quasiperiodic oscillations featuring two-dimensional torus doubling bifurcations, Technical physics letters, 31, 853-855 (2005)

34. Kuznetsov A.P., Kuznetsov S.P., Stankevich N.V., A simple autonomous quasiperiodic self-oscillator, Communications in Nonlinear Science and Numerical Simulation, 15, 1676-1681 (2010)
35. Kuznetsov A.P., Kuznetsov S.P., Mosekilde E., Stankevich N.V., Co-existing hidden attractors in a radiophysical oscillator system, Journal of Physics A: Mathematical and Theoretical, 48, 125101 (2015)
36. Wiggers V., Rech P.C. Chaos, Periodicity, and Quasiperiodicity in a Radio-Physical Oscillator, International Journal of Bifurcation and Chaos, 27, 1730023 (2017)
37. Ermentrout B., Simulating, analyzing, and animating dynamical systems: a guide to XPPAUT for researchers and students (Vol. 14). Siam. (2002)
38. Grebogi C., Ott E., Yorke J.A., Chaotic attractors in crisis, Phys. Rev. Lett. 48, 15071510 (1982)